SIMULATION OF RIVER MORPHOLOGY DEVELOPMENT ACCOUNTING FLEXIBILITY OF RIPARIAN VEGETATION

RUNYE ZHU
Department of Civil Engineering, Nagoya University, Nagoya, Japan, zhu.runye@h.mbox.nagoya-u.ac.jp

RYOTA TSUBAKI
Department of Civil Engineering, Nagoya University, Nagoya, Japan, rtsubaki@civil.nagoya-u.ac.jp

ABSTRACT

The interaction between riparian vegetation and river morphology development has attracted the attention of researchers for many years and significant progress has been made in numerical simulations. In previous 2D numerical simulations of river morphology development, according to a thorough literature search, the effects of vegetation flexibility has not yet been studied. The objectives of this study were to specify how and how much vegetation flexibility can influence river morphological development. We combined the Delft3D morphodynamic model with a model predicting vegetation dynamics and reconfiguration under the influence of shallow water flow. In the model, vegetation can colonize dry places during low discharge and can be destroyed by scouring and burial during floods. To clarify the effect of flexibility, rigid and flexible vegetation were compared. We determined that: 1) flexibility impacts averaged water depth and active river width, and, thus, influences river morphology over the long term; 2) flexible vegetation can elevate the river bed faster than rigid vegetation, and rivers with flexible vegetation yield a larger area with higher elevation; and 3) flexible vegetation is more easily destroyed by flooding than rigid vegetation, and can affect habitat areas in simulations. Since vegetation flexibility can generate non-negligible effects on river morphology development over long term, our results indicate that vegetation flexibility should be taken into consideration in river morphology simulations.

Keywords: flexible vegetation, river morphology, numerical simulation

1. INTRODUCTION

The importance of riparian vegetation on fluvial morphological vegetation has been gradually recognized by researchers (Camporeale et al., 2013; Gurnell, 2014; Hickin, 1984; Solari et al., 2016; Tal & Paola, 2007; Tsujimoto & Kitamura, 1998). Vegetation can reduce bed shear stress, increase sediment deposition, and stabilize the river bank (Millar, 2000; Nepf, 2012). As a result, the presence of vegetation changes river morphology. Vegetation may increase the sinuosity of a meandering river and has the potential to alter a multi-thread river into a single-thread river (Perucca et al., 2007; Tal & Paola, 2007). Due to its impact on river morphology and ecology, vegetation is also considered to be a kind of river system engineer (Gurnell, 2014).

The effect of vegetation on river morphology has previously been evaluated using numerical models. Previous studies have shown that riparian vegetation can significantly influence river morphological development (Bertoldi et al., 2014; Crosato & Saleh, 2011; Murray & Paola, 2003; Oorschot et al., 2016). Crosato and Saleh (2011) investigated the influence of floodplain vegetation and floodplain pioneer vegetation on braiding river morphological change. In the simulation of Crosato and Saleh (2011), vegetation was considered by changing river bed roughness. Vegetation colonization was also considered and vegetation was assumed to be rigid. Results obtained from the simulation indicated that floodplain vegetation has the potential to make a braiding river into a single thread river. Bertoldi et al. (2014) proposed a model that accounted for the environmental preference of different vegetation species and determined that even small changes in vegetation composition or water availability may result in the river changing from vegetated to unvegetated or vice versa. The Bertoldi et al. (2014) model assumed vegetation biomass and bed roughness as an explanatory parameter. Although modeling of interaction between vegetation and fluvial morphological changes has yielded great progress over the past fiew years (Oorschot et al., 2016; Weisscher et al., 2019), flexibility has not normally been considered in numerical morphology models. In both experimental (Chen et al., 2012) and numerical studies (Marjoribanks et al., 2019; Verschoren et al., 2016), the flexibility of vegetation has been found to alter local hydrodynamics and sediment transport. The local effect of vegetation flexibility may propagate to reach scale morphological changes, although such aspects have not yet

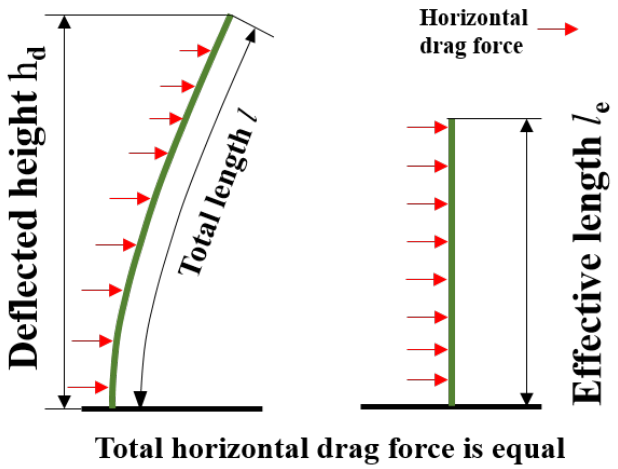

Figure 1. Deflected height and effective length.

been studied . For our work, we focused on the impact of vegetation flexibility on river morphological change.

We developed a model to predict deformation, colonization, and mortality of flexible vegetation and combined it to the morphodynamic model Delft3D. Vegetation effects were reflected by adding source terms to the momentum equations, calculated using the reduction factor approach (De Jong, 2005). The method proposed by Luhar and Nepf (2011) was applied for estimating the deformation of flexible vegetation, which includes bending and vegetation height reduction.

2. METHODS

2.1 Vegetation Deformation Modeling

One feature of flexible vegetation is that vegetation bends when confronted by water flow. The bending of vegetation reduces vegetation height. The method proposed by Luhar and Nepf (2011) is used to calculate the deformation of flexible vegetation. A simplified model has been accepted for calculating deformation. In the Luhar and Nepf (2011) model, vegetation is considered as a blade with a small thickness, incoming flow is assumed uniform over depth, and form drag is the dominant hydrodynamic force. Friction of a blade is ignored. The drag coefficient is constant and vegetation is totally submerged. Details may be found in Luhar and Nepf (2011).

The deflected height of vegetation can be numerically calculated by considering the force balance between the blade restoring force, the flow drag force, and the buoyancy force. To describe the drag reduction induced by vegetation deformation, Luhar and Nepf (2011) introduced the effective blade length, l_e. The force exerted on the flexible blade is equal to a rigid, vertical blade that has a length equal to l_e (Fig. 1). An empirical formula is given for evaluating the effective length, shown as follows:

$$\frac{l_e}{l} = 1 - \frac{\left(1 - 0.9\mathrm{Ca}^{-1/3}\right)}{1 + \mathrm{Ca}^{-3/2}\left(8 + B^{3/2}\right)}. \tag{1}$$

In above formula, $\mathrm{Ca} = \frac{1}{2}\frac{\rho C_D b U^2 l^3}{EI}$ is the Cauchy number and $B = \frac{\Delta\rho g b t l^3}{EI}$ represents the influence of the buoyancy force, where C_D is the drag coefficient, ρ is the water density, b is the blade width, U is the incoming flow velocity, l is the standing blade length, E is Young's modulus, I is the second momentum of area, and $\Delta\rho$ is the difference between water density and vegetation density. Since its value is relatively small, B is set to 0.

We additionally used an approximated hyperbolic decline curve for fitting the deflected height, h_d, obtained by the method of Luhar and Nepf (2011):

$$\frac{h_d}{l} = \alpha(1 + \beta\mathrm{Ca}/\epsilon)^\theta, \tag{2}$$

where α, β, ϵ, and θ are constants that depend on buoyancy and Young's modulus. Later in the paper, h_d is used for estimating bed roughness. We determined that when the Cauchy number, Ca, is extremely small, the non-dimensional deflected height, h_d, and effective length, l_e, are larger than 1, which is unrealistic. In such situations, we forced the non-dimensional deflected height and the effective length to be 1.0.

2.2 Numerical hydro-morphology model on a vegetated channel

The numerical simulation was performed with Delft3D (Lesser et al., 2004). Two-dimensional, depth-averaged shallow water equations were solved by coupling sediment transport and the morphology development model. Details regarding the hydrodynamic and morphology model may be found in the manual of Delft3D (Deltares, 2018).

The effects of vegetation on water flow can be considered by adding a source term to the momentum equations within the depth-averaged model. For submerged vegetation, using the depth-averaged velocity overestimates the bed shear stress, thus leading to an overestimation for sediment flux. Therefore, a reduction factor approach (De Jong, 2005) was used that modifies the bed roughness, C, as follows:

$$C = C_{\mathrm{b}} + \frac{\sqrt{g}}{\kappa} \ln\left(\frac{h}{h_v}\right) \sqrt{1 + \frac{C_{\mathrm{D}} m D h_v C_{\mathrm{b}}^2}{2g}}. \tag{3}$$

In Eq. (3), C is the Chezy roughness coefficient, C_{b} is the bare bed roughness, and m is the vegetation density that indicates the number of stems per unit area. D is the representative length of the vegetation stem that represents the width of a blade. h is the water depth. h_v is the height of rigid vegetation, equivalent to l in Section 2.1 for rigid vegetation. κ is the von Kárman constant, 0.4 for our research. g is the gravitational acceleration.

A source term $-\frac{\lambda}{2}u^2$ is added to the momentum equations, where the coefficient λ is calculated by:

$$\lambda = C_{\mathrm{D}} m D \frac{h_v}{h} \frac{C_{\mathrm{b}}^2}{C^2}. \tag{4}$$

The reduction factor approach is a modification of the formula proposed by Baptist et al. (2007). Although the original method proposed by Baptist et al. (2007) was based on a rigid analogy of vegetation, it works reasonably well as long as the deflected vegetation height is known when vegetation is flexible (Vargas-Luna et al., 2015; Verschoren et al., 2016). According to the description in Section 2.1, the deflected height of flexible vegetation can be calculated from the Ca number. Although, the vegetation height, h_v, in Eq. (3) can be replaced by the deflected height, h_d, it is more reasonable to replace h_v in Eq. (3) by the effective length, l_e, since the square root portion in Eq. (3) represents the resistance induced by the river bed and the vegetation canopy (Verschoren et al., 2016). In a similar manner, we replaced h_v in Eq. (4) by l_e. Therefore, modifications were made to Eqs. (3) and (4) and we obtained:

$$\lambda = C_{\mathrm{D}} m D \frac{l_e}{h} \frac{C_{\mathrm{b}}^2}{C^2}, \text{ and} \tag{5}$$

$$C = C_{\mathrm{b}} + \frac{\sqrt{g}}{\kappa} \ln\left(\frac{h}{h_d}\right) \sqrt{1 + \frac{C_{\mathrm{D}} m D l_e C_{\mathrm{b}}^2}{2g}}. \tag{6}$$

Equation (6) was used to calculate the bed shear stress and Eq. (5) was added to the momentum equations in order to calculate the drag force exerted on vegetation.

2.3 Population dynamics model of vegetation

A simple model was developed in order to describe vegetation dynamic processes, including colonization and mortality of vegetation. The vegetation model used in our work was inspired by the dynamic vegetation model proposed by Oorschot et al. (2016). The model simulation was separated into a so-called morphological step and an ecological step, and the vegetation dynamic was updated within the ecological step.

Major differences between our model and that of Oorschot et al. (2016) are: 1) within the ecological step of our model the deformation of flexible vegetation was updated based on the method in Section 2.1 and 2) our model only considered one type of vegetation. The following three processes related to vegetation were determined within the ecological steps: 1) the colonization of vegetation during a certain time window; 2) the destruction of vegetation due to scouring, burial and hypoxia; and 3) an update of vegetation deformation due to vegetation flexibility.

In our model, vegetation seeds were assumed to be well-supplied and the bare ground grid with a water depth

smaller than a certain value of h_c was instantly covered by vegetation during the low discharge period. In the simulation, when sediment deposition is deeper than the initial vegetation height, vegetation is regarded as buried and is removed from the grids. Similar to burial, when erosion between two morphological steps is larger than the specified root depth, vegetation is removed from the grids. At the beginning of every flood, if water depth is greater than the value of $h_{hypoxia}$ within a vegetated grid, vegetation is removed from the simulation due to the death of the root system. In the flexible vegetation case, the deformation of vegetation is calculated every hour. In the deformation update, if the velocity is not strong enough for flexible vegetation to be fully submerged, vegetation is considered to be emergent. For emergent vegetation, deflected height and effective length are replaced by the local water depth.

3. SIMULATION SETTING

Profiles of the simulation domain for our research were determined based on the Kizu River (Japan). The domain is 10,000 m in the streamwise direction and $400\,\mathrm{m}$ in the spanwise direction. To minimize the influence of both upstream and downstream boundaries, a domain of $1000\,\mathrm{m} < x < 9000\,\mathrm{m}$ was used in the analysis. In the simulation, free slip boundary conditions were applied to the side walls.

The initial bed of our simulation was a compound channel. The depth of the main channel was $1\,\mathrm{m}$ and the width was $200\,\mathrm{m}$ (Fig. 2). The grid size was set to $10 \times 10\,\mathrm{m}^2$. The slope of the simulation domain was 1/1140 and the sediment diameter D_{50} was $0.004\,\mathrm{m}$ (Takebayashi & Egashira, 2001). The Chezy coefficient, C, of the bare bed was $60\,\mathrm{m}^{1/2}\,\mathrm{s}^{-1}$, estimated by $C = 18\log(12H/k_s)$ where H is the representative water depth and k_s is the equivalent geometrical roughness of Nikuradse. A summary of the simulation parameters is provided in Table 1.

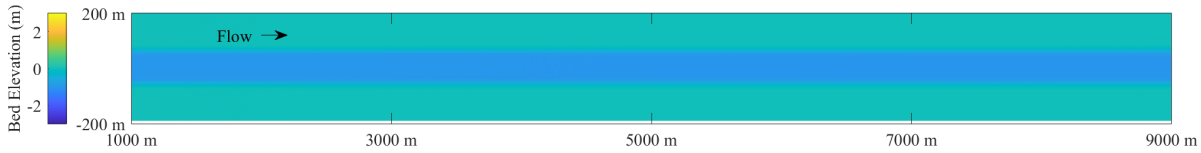

Figure 2. Initial bed elevation.

The hydrograph used in the simulation is provided in Fig. 3. Flooding occurs once per year and is considered to last for 24 hours with a discharge of Q_{max}. Low discharge is Q_{min}. Maximum discharge was set based on the research of Takebayashi and Egashira (2001). However, since our main goal was to investigate the effects of flexibility rather than to reproduce actual river morphology, flood duration differed from reality, and we simplified the hydrograph. Q_{max} was set to $2000\,\mathrm{m}^3\,\mathrm{s}^{-1}$ (Takebayashi & Egashira, 2001) and Q_{min} was set to $30\,\mathrm{m}^3\,\mathrm{s}^{-1}$. Since major changes in river morphology occur during flooding periods, to reduce simulation time, the simulation skipped the period during the low stage. A morphological scale factor was used to speed up morphological change.

Two types of vegetation were tested. One was rigid and the other flexible. For rigid vegetation, the effective length does not change with drag force. Vegetation geometry is simplified as a single blade. Parameters are provided in Table 2. The parameters of vegetation geometry were chosen to be relatively arbitrary. However the elastic modulus of flexible vegetation was the same as for *Phragmites japonica* measured within the Kizu River (Tsujimoto & Kitamura, 1998). The drag coefficient C_D of the blade was set to 1.95 (Vogel, 1996). The root depth for both types of vegetations was $0.5\,\mathrm{m}$. The buoyancy of flexible vegetation was neglected (Luhar & Nepf, 2011). Simulation cases are provided in Table 3.

4. RESULTS

4.1 River morphology

Without vegetation, the initial compound channel evolves into multiple row bars (Fig. 4). The river morphology evolutions of a river with rigid and flexible vegetation are provided in Figs. 5 and 6, respectively. We found that the bar mode in the river without vegetation does not significantly change with time. In the flexible vegetation case, after 20 floods, we still observed a mid-channel bar in the upstream. However, the transformation from multiple row bars to alternate bars was still observed in the downstream. At the end of the simulation, the river with rigid vegetation evolved into a single-thread river. In the river with rigid vegetation, the average wavelength of the alternate bar (Fig. 6) was shorter than that for the flexible case (Fig. 5).

Table 1. Channel parameters

Items	Values
Simulation domain width	400 m
Simulation domain length	10 000 m
Channel slope	0.000877
D_{50}	0.004 m
Q_{max}	2000 $m^3 s^{-1}$
Q_{min}	30 $m^3 s^{-1}$
Flood events number	20
Morphological scale factor	10

Table 2. Vegetation parameters

Items	Values
Vegetation height l	0.5 m
Blade width b	0.01 m
Blade thickness t	0.001 m
Root depth	0.5 m
Drag coefficient C_D	1.95
Colonization water depth h_c	0.1 m
Hypoxia water depth $h_{hypoxia}$	0.2 m

Table 3. Simulation cases

Case No.	Case name	Discharge (m^3/s)	Elastic modulus (Pa)	Vegetation density (stems/m^2)
Case I	Q20d40F1	2000	9×10^9	40
Case II	Q20d40R	2000	∞	40
Case III	Q20d40N	2000		0

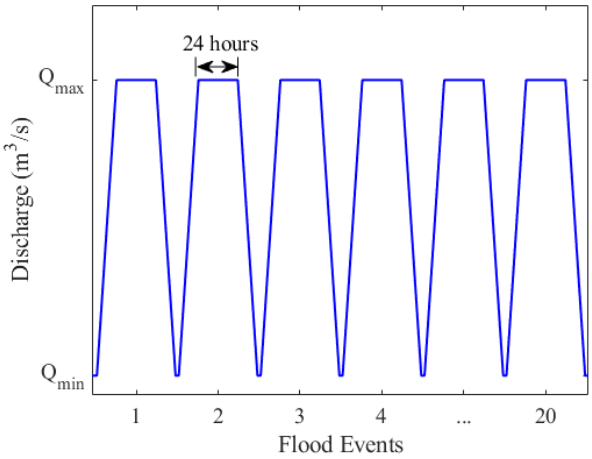

Figure 3. Hydrograph

4.2 River depth and width

Flexibility also influences spatial averaged water depth during floods (Fig. 7a). Here, the average water depth is defined as the ratio of the total water volume to the total wet area. The average water depth for the flexible vegetation case is shallower than that for the rigid vegetation case but deeper than the river without vegetation, implying that the global resistance induced by flexible vegetation is not as large as that for rigid vegetation. Average water width is calculated as the ratio of the total wet area to the simulation area length. Results for this calculation are provided in Fig. 7b. Since during floods the average water width almost requires maximum river width for all three cases, flexibility does not have a significant influence on river width. Similar to average water width, average active water width is the ratio of active river bed (the river bed with bedload transport) area to the domain length. In the case without vegetation, the river has the widest active width and almost requires the entire river width (Fig. 7c). The river with rigid vegetation yields the smallest active water width.

4.3 Bed elevation evolution and distribution

The effect of flexibility on bed elevation can be observed based on the time history of bed elevation evolution (Fig. 8). We compared the time history of the 5th, 50th and 95th percentile elevation (often referred to as the p5, p50, and p95 elevation, respectively) for three cases. Since the morphological scale factor is used, results shown in Figs. 8 and 9 represent the trend over the long term. Without vegetation, variation of the p5, p50, and p95 elevations after the 8th flood are smaller than those in vegetated rivers (Figs. 8a to 8c). For both the flexible and rigid cases, the p5 elevation decreases with time. The difference in the p5 elevation between the flexible and rigid cases becomes significant after around the 13th flood (Fig. 8a). Variation of the p50 elevation with time for the flexible case is higher than for the rigid case (Fig. 8b). For the majority of simulation time, the p50 elevation in the flexible case was higher than for the rigid case. The p95 elevation increased and reached an almost constant

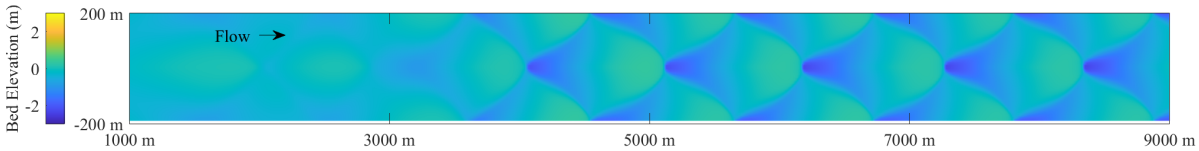

Figure 4. The bed elevation of Case III after the 20th flood.

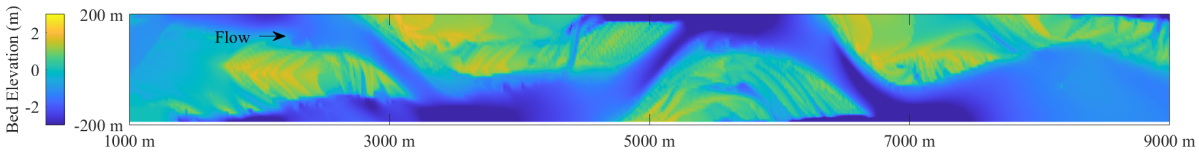

Figure 5. The bed elevation of Case I after the 20th flood.

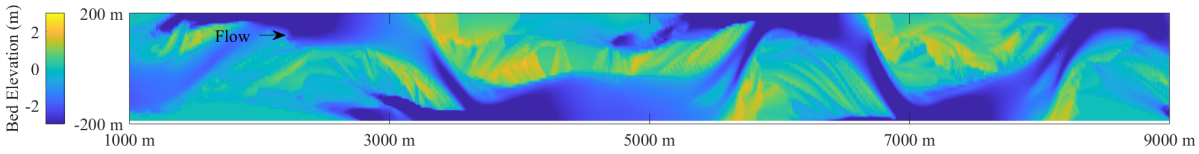

Figure 6. The bed elevation of Case II after the 20th flood.

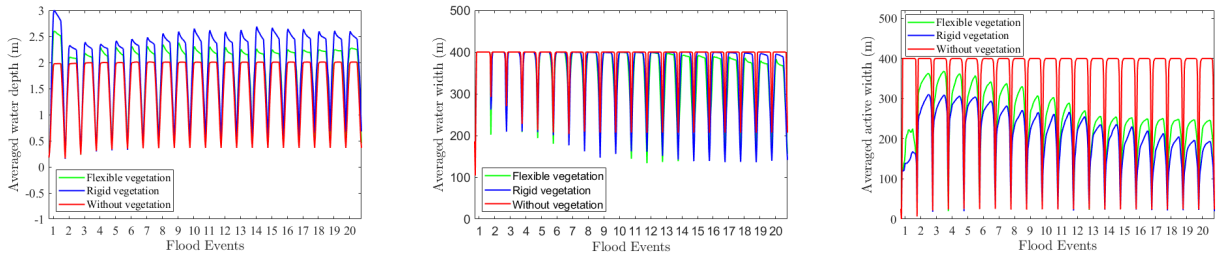

(a) Average water depth (b) Average water width (c) Average active water width

Figure 7. Time history of the spatial averaged water depth, water width and active water width.

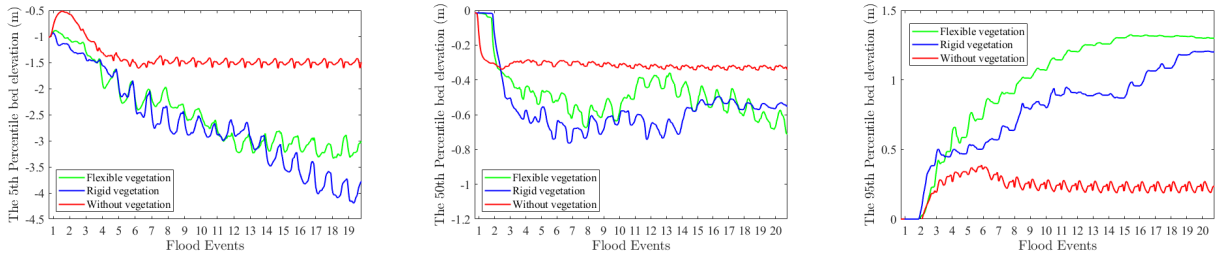

(a) 5th percentile bed elevation (b) 50th percentile bed elevation (c) 95th percentile bed elevation

Figure 8. The time history of bed elevation percentiles.

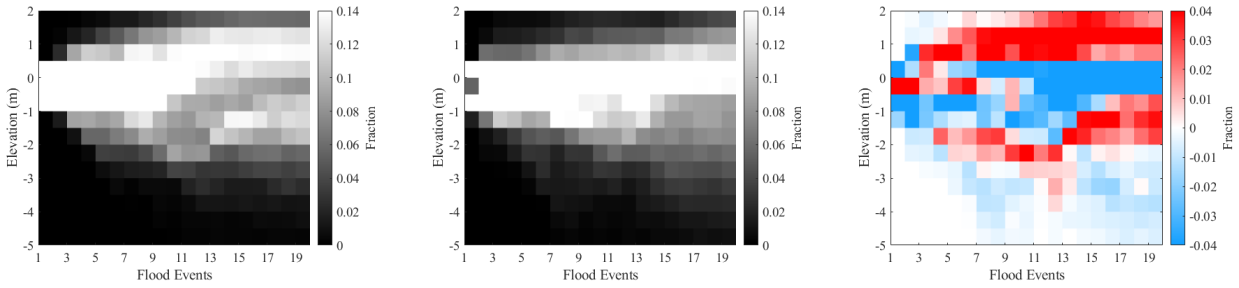

(a) Time history of the Case I elevation histogram (b) Time history of the Case II elevation histogram (c) Differences between two elevation histograms

Figure 9. The time history of elevation histogram and their differences

value for both the flexible and rigid cases (Fig. 8c). However, p95 elevation for the flexible case increased faster than for the rigid case, and final elevation in the flexible case was slightly higher than for the rigid case.

The flexibility of vegetation also influenced the elevation histogram in the river. The time history of the elevation

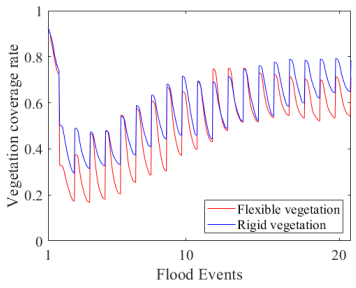

(a) Vegetation coverage rate change during the simulation

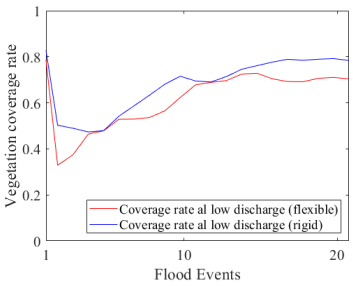

(b) Vegetation coverage at low discharge

Figure 10. Vegetation coverage rate

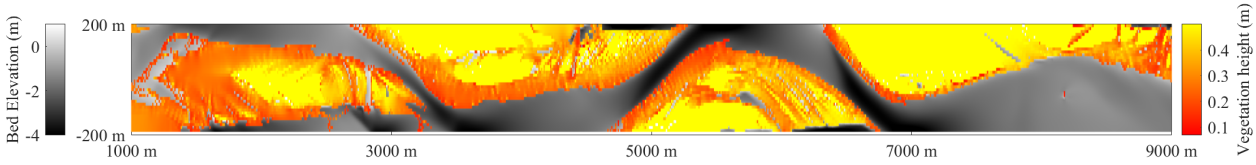

Figure 11. Vegetation cover at the beginning of the 20th flood.

histogram at the end of the max discharge period for each flood event is provided in Figs. 9a and 9b. Prior to the 11th flood, the fraction of elevation between $-1.5\,\mathrm{m}$ to $0.5\,\mathrm{m}$ was the greatest. Following the period around the 11th flood, the elevation histogram became different. For the flexible case, the fraction of elevation above $0.5\,\mathrm{m}$ became larger following the 11th flood (Fig. 9a). For the rigid case, the fraction of elevation below $-1.0\,\mathrm{m}$ decreased. As compared to the flexible case, the fraction of elevation above $0.5\,\mathrm{m}$ did not significantly increase. Fig. 9c provides the difference elevation histogram distribution between the two cases, which was obtained by subtracting the rigid case elevation distribution from the flexible case. For the flexible case, the area fraction of the river bed with a higher elevation was larger than for the rigid case.

4.4 Vegetation coverage

The time histories of the vegetation coverage rates for rigid and flexible vegetation are provided in Fig. 10a. In both cases, the area of vegetation first decreased and then increased. The rapid decrease in the vegetation coverage rate during the first two floods is attributed to the influence of the initial bed. Reduction in coverage during the flood period was smaller for the rigid case, implying that rigid vegetation may have a stronger resistance to flooding. The vegetation coverage rate in the river with flexible vegetation was 10% less than the river with rigid vegetation, suggesting the flexibility can affect the vegetation habitat area. Vegetation distribution at the beginning of the 20th flood is provided in Fig. 11; and indicates that on bar tops, a reduction of vegetation height was limited. The result suggests that the significance of flexibility gradually decreases with the growth of bars.

5. CONCLUSIONS

A model for predicting river morphology development by accounting for vegetation flexibility is proposed. Although relatively simple, this model provides information regarding the potential effects of vegetation flexibility on river morphology. The results of our numerical modeling study indicate that, in comparison to the river with rigid vegetation, the river with flexible vegetation has a shallower average water depth and a wider average active width. Therefore, the river with flexible vegetation has a larger width-to-depth ratio than the river with rigid vegetation , and this may account for the different river morphology over the long term in the two rivers. We also found that the area of river bed with a higher elevation is larger in the river with flexible vegetation, whereas in the river with rigid vegetation the area is smaller. The time history of vegetation coverage rates indicates that flexible vegetation is easily destroyed by flooding and that vegetation flexibility influences its habitat area. More in-depth research is needed to better understand the effects of vegetation flexibility.

REFERENCES

Baptist, M., Babovic, V., Rodríguez Uthurburu, J., Keijzer, M., Uittenbogaard, R., Mynett, A., & Verwey, A. (2007). On inducing equations for vegetation resistance. *Journal of Hydraulic Research*, *45*(4), 435–450.

Bertoldi, W., Siviglia, A., Tettamanti, S., Toffolon, M., Vetsch, D., & Francalanci, S. (2014). Modeling vegetation controls on fluvial morphological trajectories. *Geophysical Research Letters*, *41*(20), 7167–7175.

Camporeale, C., Perucca, E., Ridolfi, L., & Gurnell, A. (2013). Modeling the interactions between river morphodynamics

and riparian vegetation. *Reviews of Geophysics*, *51*(3), 379–414.
Chen, S.-C., Kuo, Y.-M., & Yen, H.-C. (2012). Effects of submerged flexible vegetation and solid structure bars on channel bed scour. *International Journal of Sediment Research*, *27*(3), 323–336.
Crosato, A., & Saleh, M. S. (2011). Numerical study on the effects of floodplain vegetation on river planform style. *Earth Surface Processes and Landforms*, *36*(6), 711–720.
De Jong, J. (2005). Modelling the influence of vegetation on the morphodynamics of the river Allier, Delft. *Delft University of Technology, Faculty of Civil Engineering and Geosciences, Section Hydraulic Engineering. M. Sc. thesis*.
Deltares. (2018). *Delft3d-FLOW User Manual*.
Gurnell, A. (2014). Plants as river system engineers. *Earth Surface Processes and Landforms*, *39*(1), 4–25.
Hickin, E. J. (1984). Vegetation and river channel dynamics. *Canadian Geographer/Le Géographe canadien*, *28*(2), 111–126.
Lesser, G. R., Roelvink, J. v., Van Kester, J., & Stelling, G. (2004). Development and validation of a three-dimensional morphological model. *Coastal Engineering*, *51*(8-9), 883–915.
Luhar, M., & Nepf, H. M. (2011). Flow-induced reconfiguration of buoyant and flexible aquatic vegetation. *Limnology and Oceanography*, *56*(6), 2003–2017.
Marjoribanks, T., Lague, D., Hardy, R., Boothroyd, R., Leroux, J., Mony, C., & Puijalon, S. (2019). Flexural rigidity and shoot reconfiguration determine wake length behind saltmarsh vegetation patches. *Journal of Geophysical Research: Earth Surface*.
Millar, R. G. (2000). Influence of bank vegetation on alluvial channel patterns. *Water Resources Research*, *36*(4), 1109–1118.
Murray, A. B., & Paola, C. (2003). Modelling the effect of vegetation on channel pattern in bedload rivers. *Earth Surface Processes and Landforms*, *28*(2), 131–143.
Nepf, H. M. (2012). Hydrodynamics of vegetated channels. *Journal of Hydraulic Research*, *50*(3), 262–279.
Oorschot, M. v., Kleinhans, M., Geerling, G., & Middelkoop, H. (2016). Distinct patterns of interaction between vegetation and morphodynamics. *Earth Surface Processes and Landforms*, *41*(6), 791–808.
Perucca, E., Camporeale, C., & Ridolfi, L. (2007). Significance of the riparian vegetation dynamics on meandering river morphodynamics. *Water Resources Research*, *43*(3).
Solari, L., Van Oorschot, M., Belletti, B., Hendriks, D., Rinaldi, M., & Vargas-Luna, A. (2016). Advances on modelling riparian vegetation-hydromorphology interactions. *River Research and Applications*, *32*(2), 164–178.
Takebayashi, H., & Egashira, S. (2001). Formative process and domain of a self-formed stream channel. *Doboku Gakkai Ronbunshu*, *2001*(677), 75–86.
Tal, M., & Paola, C. (2007). Dynamic single-thread channels maintained by the interaction of flow and vegetation. *Geology*, *35*(4), 347–350.
Tsujimoto, T., & Kitamura, T. (1998). Study on flow over flexible vegetation-covered bed. *Doboku Gakkai Ronbunshu*, *1998*(607), 29–44.
Vargas-Luna, A., Crosato, A., & Uijttewaal, W. S. (2015). Effects of vegetation on flow and sediment transport: comparative analyses and validation of predicting models. *Earth Surface Processes and Landforms*, *40*(2), 157–176.
Verschoren, V., Meire, D., Schoelynck, J., Buis, K., Bal, K. D., Troch, P., … Temmerman, S. (2016). Resistance and reconfiguration of natural flexible submerged vegetation in hydrodynamic river modelling. *Environmental Fluid Mechanics*, *16*(1), 245–265.
Vogel, S. (1996). *Life in moving fluids: the physical biology of flow*. Princeton University Press.
Weisscher, S. A., Shimizu, Y., & Kleinhans, M. G. (2019). Upstream perturbation and floodplain formation effects on chute cutoff-dominated meandering river pattern and dynamics. *Earth Surface Processes and Landforms*, *44*(11), 2156–2169.